High thermoelectric figure-of-merit in Sb2Te3/Ag2Te bulk composites as Pb-free p-type thermoelectric materials

SCHOLARONE™
Manuscripts

Journal Name

ARTICLE

High thermoelectric figure-of-merit in Sb_2Te_3/Ag_2Te bulk composites as Pb-free *p*-type thermoelectric materials

Min Ho Lee,[a] Ka-Ryeong Kim,[a] Jong-Soo Rhyee,[a,*] Su-Dong Park,[b] and G. Jeffrey Snyder[c]

We investigated the thermoelectric properties of the Sb_2Te_3/Ag_2Te (ST/AT) composites with molar ratios of ST/AT = 1/1, 2/1, 4/1, 8/1, 16/1, and 32/1. The extrinsic composites, synthesized by wet ball milling of two separate powders of Sb_2Te_3 and Ag_2Te, are differentiated with intrinsic composites by high temperature phase separation because of the low temperature synthesis process. The thermoelectric properties of the composites show systematic behaviour of decreased electrical and thermal conductivities with increasing Ag_2Te dispersion concentration. The ST/AT = 1/1 composite exhibits extremely low lattice thermal conductivity with high power factor over a wide temperature range, resulting in a high *ZT* value of 1.5 at 700 K, which is a significantly enhanced value of *ZT* compared with those of other Pb-free *p*-type chalcogenide thermoelectric materials.

1. Introduction

Thermoelectric (TE) materials have been attracting attention because of possible applications in fields such as solid state cooling and waste heat power generation. The efficiency of a TE generator requires a high dimensionless figure-of-merit $ZT = S^2\sigma T/\kappa$, where S, σ, T, and κ are the Seebeck coefficient, electrical conductivity, absolute temperature, and thermal conductivity, respectively. Recent investigations have reported progressively increased thermoelectric performance *ZT* in PbTe based materials; for example, Fermi level tuning at the resonant level in Na-doped PbTe (1.5 at 773 K),[1] convergence of band structures in $PbTe_{1-x}Se_x$ (1.8 at 850 K),[2] and hierarchical microstructure control in an SrTe- and Na-doped PbTe system (2.2 at 915 K).[3] Exceptionally high *ZT* materials ($ZT \geq 2.0$) were followed by the nano- and micro-structure modulation.[4,5]

Even though PbTe based materials are promising candidate for waste heat power generation, such as space application, the environmentally hazardous nature of Pb can cause limitations in terms of widespread application of PbTe based materials. As a Pb-free thermoelectric material, $(GeTe)_x(AgSbTe_2)_{100-x}$, which is called TAGS-m, has been studied since the early 1960s[6-8] and $(GeTe)_{1-x}[(Ag_2Te)_{1-y}(Sb_2Te_3)_y]_x$.[9] Recently, Dy-doped TAGS-85 has been found to have a high *ZT* value of 1.5 at 750 K.[10] The high thermoelectric performance of TAGS may be related with the crystallographic transformation from a high-temperature cubic to a low-temperature rhombohedral polymorph.[11]

The matrix of the TAGS, $AgSbTe_2$ compound is promising for use in *p*-type thermoelectric materials in the mid-temperature range.[12]

The ternary Ag-Sb-Te system undergoes a eutectic reaction as follows: Liquid $\rightarrow$ $AgSbTe_2$ + Ag_2Te + δ-Sb_2Te. Because of the eutectic decomposition, the quaternary melt of the Pb-Ag-Sb-Te system, which is known as the LAST system, exhibits a dendrite or phase segregated morphology.[13] It is well known that phase separated morphologies are beneficial in reduction of lattice thermal conductivity by interfacial phonon scattering.[14,15] By using the phase transformation Ag_2Te + $AgSbTe_2$ $\leftrightarrow$ Ag_2Te + Sb_2Te_3, the composite with phase separation showed high thermoelectric performance around *ZT* 1.0 ~ 1.3.[16,17], The intrinsic thermodynamic phase separation of Ag_2Te + Sb_2Te_3 at the temperature of 360 °C can cause thermal instability of thermoelectric properties in the $AgSbTe_2$ compound.

There are two different strategies for fabricating nano- or micro-structured composites. One is metallurgical phase separation [18] or precipitation;[19] the other is the synthesis of an artificial composite.[20,21] Here, we explore the thermoelectric properties of the composites of Sb_2Te_3/Ag_2Te (ST/AT) in systematic variations of ST/AT = 1/1, 2/1, 4/1, 8/1, 16/1, and 32/1 molar ratios. The extrinsic composite fabricated by mechanical ball milling of separate mixtures of Sb_2Te_3 and Ag_2Te powders can show improved thermal stability because of the low temperature synthesis of the composite. We achieved high thermoelectric figure-of-merit *ZT* of 1.5 at 700 K in the composite due to the decreased thermal conductivity caused by grain boundary phonon scattering. In spite of the *p*-type Sb_2Te_3 and *n*-type Ag_2Te composites, the Seebeck coefficients were found not to be degraded by the *p-/n*-composite, preserving the high electrical conductivity. The high *ZT* value with Pb-free elements should have a

significant impact on the field of environmentally friendly waste heat power generation.

2. Experimental

We synthesized the Sb_2Te_3 and Ag_2Te ingots by melting using high purity Ag (99.999 %), Sb (99.999 %), and Te (99.999 %) granules. For the synthesis of Sb_2Te_3, the evacuated quartz ampoules were melted at 800 °C for 24 h and slowly cooled to room temperature with a cooling rate of 10 °C/h.

The Ag_2Te ingots were melted at 1000 °C for 24 h in the evacuated quartz ampoules, slowly decreased the temperature to 500 °C, and water quenching. Sb_2Te_3 and Ag_2Te ingots were pulverized by hand grinding for 6 h in an agate mortar. The pulverized powders were mixed and stirred in an *n*-hexane solution. The dried powder mixtures of Sb_2Te_3/Ag_2Te (ST/AT = 1/1, 2/1, 4/1, 8/1, 16/1, and 32/1) were sintered by hot press sintering at 350 °C with application of uniaxial pressure of 70 MPa for 1 hour.

The phase identification and structural characterization of the composites were performed by powder X-ray diffraction (XRD) with Cu Kα radiation. The microstructure and relative concentration of elements were determined by scanning electron microscopy (SEM) and energy dispersive X-ray spectroscopy (EDX) measurements (JEOL, Japan). The Seebeck coefficient and electrical resistivity were determined via a four point probe method using a thermoelectric measurement system (ZEM-3 ULVAC, Japan). The thermal conductivity was obtained by $\kappa = \rho_s C_p \lambda$, where ρ_s, C_p, and λ are the sample density, specific heat measured by the physical property measurement system (PPMS, Quantum Design, USA), and thermal diffusivity measured by a laser flash method, respectively.

3. Results and Discussion
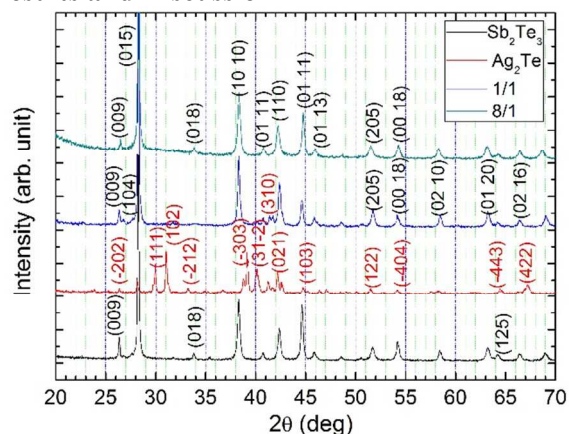
Fig. 1 Powder X-ray diffraction patterns of the Sb_2Te_3, Ag_2Te, and Sb_2Te_3/Ag_2Te (ST/AT) composites with molar ratios of (ST/AT = 1/1 and 8/1). The red miller indices represent the Ag_2Te.

Figure 1 presents the powder X-ray diffraction patterns of the hot-press sintered ST/AT composite samples of ST/AT = 1/1 and 8/1 together with the major diffraction peaks of Sb_2Te_3 and Ag_2Te single phase compounds. The diffraction peaks of the Sb_2Te_3 (black, 1st from the bottom) and Ag_2Te (red, 2nd from the bottom) show single phases of rhombohedral ($R\bar{3}m$) Sb_2Te_3 and monoclinic ($P2/n$) α-

Ag_2Te crystal structures, respectively. The mixed phases of Sb_2Te_3/Ag_2Te = 1/1 (blue, 3rd from the bottom) and ST/AT = 8/1 (sky blue, the top line) show that the major peak corresponds to Sb_2Te_3 with small Ag_2Te impurity peaks. The lattice parameters of Sb_2Te_3, Ag_2Te and their composites with molar ratios of (ST/AT = 1/1, 2/1, 4/1, 8/1, 16/1, and 32/1) are presented in Table 1.

		a (Å)	b (Å)	c (Å)
Single Phases	Sb_2Te_3	4.279	-	30.481
	Ag_2Te	8.165	8.935	8.061
Sb_2Te_3 (ST/AT)	1/1	4.278	-	30.467
	2/1	4.278	-	30.469
	4/1	4.278	-	30.476
	8/1	4.279	-	30.475
	16/1	4.279	-	30.479
	32/1	4.279	-	30.481

Table 1 Lattice parameters of Sb_2Te_3, Ag_2Te, and Sb_2Te_3/Ag_2Te composites with molar ratios of ST/AT = 1/1, 2/1, 4/1, 8/1, 16/1, and 32/1.

The lattice parameters of Sb_2Te_3 and α-Ag_2Te correspond to those in previous reports.[22,23] The *a*-axis lattice parameters of Sb_2Te_3 for the composite are not changed, while the *c*-axis lattice parameters are slightly increased with decreasing of the Ag_2Te mole fraction. The lattice parameters of the small mole fraction of Ag_2Te (32/1) are almost identical to those of the pristine Sb_2Te_3 compound. The lattice parameters of Ag_2Te for the composites cannot be obtained due to the small impurity peaks of the compound.

The small decrease of the *c*-axis lattice parameter, without significant change of the *a*-axis lattice parameter with increasing Ag_2Te volume fraction, implies a small solid solution reaction with Ag_2Te and Sb_2Te_3 because the *c*-axis lattice parameter of Ag_2Te is smaller than that of Sb_2Te_3. If a small amount of Ag can be incorporated in the van der Waals gap of Sb_2Te_3, the *c*-axis lattice parameters should be increased. Also, if Ag atoms substitute at the Sb, Te, or interstitial sites, the *a*- and *c*-axis lattice parameters are also increased due to the larger atomic size of Ag (160 pm) than those of Sb (145 pm) and Te (140 pm).
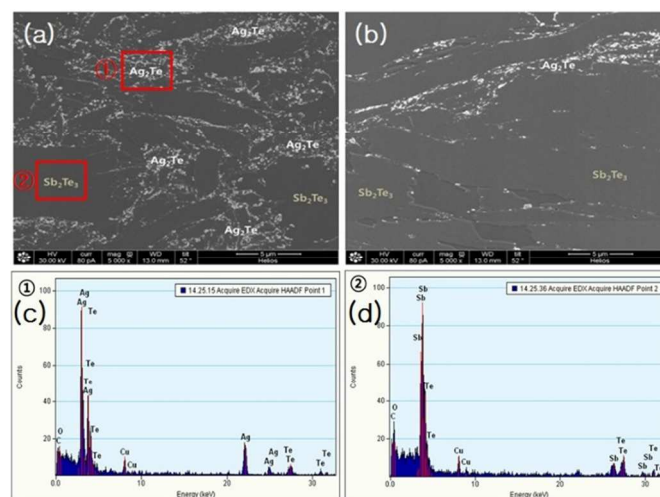
Fig. 2 Scanning electron microscopy images of Sb_2Te_3/Ag_2Te composite of ST/AT= 1/1 for perpendicular (a) and parallel direction (b) of the uniaxial pressure direction. (c) and (d) represent the energy dispersive X-ray spectroscopy data in the white Ag_2Te and grey Sb_2Te_3 regions, respectively as indicated in the red boxes of (a).

Figure 2(a) and 2(b) presents scanning electron microscope (SEM) images of the ST/AT = 1/1 composite cross-sectional and parallel directions respectively, for the uniaxial hot press direction. The mole fraction of ST/AT = 1/1 corresponds to an almost 2/1 volume fraction. Energy dispersive x-ray spectroscopy (EDX) shows that the dark and white grey regions of Fig. 2(a) and 2(b) are Sb_2Te_3 and Ag_2Te phases, as shown in Fig. 2(c) and 2(d), respectively. The Ag_2Te phase is well dispersed in the Sb_2Te_3 matrix in the cross-sectional plane across the uniaxial pressure direction of the hot press. Along the uniaxial direction, the Ag_2Te phase is not homogeneously distributed but shows striped distribution, indicating that the Ag_2Te more homogeneously dispersed across the perpendicular plane of the uniaxial pressure direction of the hot press.

When we examine many different spots of the Sb_2Te_3 region using EDX, there are no Ag peaks, as shown in Fig. 2(d). Also, the white regions in Fig. 2(a) shows only Ag and Te peaks without Sb concentration. This indicates that the Ag_2Te phase separated well from the Sb_2Te_3 matrix. Near the grain boundaries between the Sb_2Te_3 and Ag_2Te phases, a solid solution reaction can be possible; this is the result of the small decrease of the *c*-axis lattice parameters in the ST/AT composites in the powder X-ray diffraction. The grain sizes of Ag_2Te range from 200 nm to 5 μm with anisotropic dispersion. The anisotropic distribution of Ag_2Te particles implies anisotropic thermoelectric properties. Here we measured the thermoelectric properties of the composites across the uniaxial pressure direction.
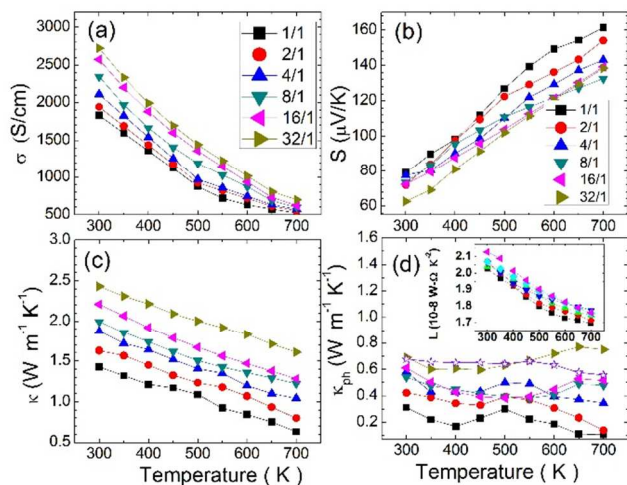
Fig. 3 Temperature-dependent thermoelectric properties of Sb_2Te_3/Ag_2Te (ST/AT) composites with molar ratios of (ST/AT = 1/1, 2/1, 4/1, 8/1, 16/1, and 32/1); Electrical conductivity (a), Seebeck coefficient (b), total thermal conductivity κ_{tot} (c), lattice thermal conductivity κ_{ph} (d), and Lorenz number $L(T)$ (inset of (d)). Star open symbol in (d) represents the lattice thermal conductivity of Sb_2Te_3.

Figure 3 shows the temperature-dependent electrical conductivity $\sigma(T)$ (a), Seebeck coefficient $S(T)$ (b), thermal conductivity $\kappa(T)$ (c), and lattice thermal conductivity $\kappa_{ph}(T)$ (d), and Lorenz number $L(T)$ (inset of (d)) of ST/AT composite with molar ratios of ST/AT = 1/1, 2/1, 4/1, 8/1, 16/1, and 32/1, measured along the vertical direction of the uniaxial hot press direction. The electrical conductivity $\sigma(T)$ shows typical metallic behaviour, as shown in Fig. 3(a), which is similar to but lower than those of the single crystalline Sb_2Te_3 (5105 S/cm).[24] The decreased electrical conductivity is due to the Ag_2Te dispersion in the polycrystalline Sb_2Te_3 matrix. The electrical transport properties of the nano-sheets of sintered Sb_2Te_3 bulk samples show typical semiconductor behaviour with an electrical conductivity value of 230 S/cm at 300 K.[25,26] The electrical conductivity values of nano-sheet sintered compounds are remarkably lower by one order of magnitude than those of bulk Sb_2Te_3 due to significant electron scattering at the nano-grain boundaries.

With increasing of the mole fraction of Ag_2Te, the electrical conductivity is decreased to 1832 S/cm (at 300 K) for the ST/AT = 1/1 composite. The electrical conductivity of the Sb_2Te_3 rich composite (ST/AT = 32/1) has a value of 2700 S/cm at 300 K, but the σ values at high temperature (700 K) are not sensitive with Ag_2Te dispersion concentration. The electrical conductivity values of α- and β-Ag_2Te were 400 S/cm and 100 S/cm, respectively, at room temperature which are both lower than that of Sb_2Te_3.[27] Therefore, it is not surprising to observe a decrease of electrical conductivity with increasing Ag_2Te dispersion concentration due to the low electrical conductivity of Ag_2Te and the grain boundary scattering of the carriers.

The Seebeck coefficients of the ST/AT composites are presented in Fig. 3(b). The $S(T)$ increases with increasing temperature, which is a typical metallic behaviour. Because of the decreased electrical conductivity, the Seebeck coefficient increases with increasing Ag_2Te dispersion concentration. The Seebeck coefficient dependence on the Ag_2Te dispersion concentration at high temperature is more significant than that of the room temperature Seebeck coefficient variation with varying of the Ag_2Te concentration. The Seebeck coefficient of the single crystalline Sb_2Te_3 compound had value of 83 μV/K along the cleavage planes and 92 μV/K along the perpendicular direction at 300 K, which is similar to the value of ST/AT = 1/1.[28] In the case of the Sb_2Te_3 nano-particle systems, the value is 210 μV/K due to low electrical conductivity.[25,26] The Seebeck coefficients of α- and β-Ag_2Te were found to be in a range from 120~170 μV/K due to the *p*-type conduction of the carriers.[27] Because the carriers are of the same type between Sb_2Te_3 and Ag_2Te, the Seebeck coefficients are not significantly degraded with increasing Ag_2Te dispersion concentrations.

From the *ab*-initio first principle band structure calculation of Sb_2Te_3, it can be seen that this is a degenerate semiconductor in which the Fermi level (E_F) is positioned near the top of the valence band maximum with a small band gap $\Delta \leq 0.1$ eV at the Γ-point.[29,30] The original electronic band structure of α-Ag_2Te is that of a zero-gap semiconductor; however there is a strong Te 4*p*-Ag 4*d* hybridization shift up to the Te 4*p*-orbital and a push down to the Ag 4*d* band, resulting in the formation of a semiconducting energy band gap; the Fermi level resides at the top of the valence band maximum.[31] The electronic band structure of β-Ag_2Te shows that the Fermi level is pinned near the conduction band minimum.[31] Even if it is well known that the band gap is overestimated in theoretical calculation, the

Fermi level shift to the conduction band minimum from α- to β-phase indicates the lower Seebeck coefficients of β-Ag_2Te than those of α-Ag_2Te.

Table 2 shows the Hall carrier concentration n_H, Hall mobility μ_H, Seebeck coefficient S, and effective mass m^* at 300 K of the Sb_2Te_3/Ag_2Te composites. For increased Ag_2Te dispersion concentration, the Hall carrier concentrations are decreased and the Hall mobilities are systematically increased. The lower Hall mobility of Sb_2Te_3 rich composite (32/1) than the μ_H value of the ST/AT = 1/1 composite implies that the systematic increase of the Hall mobility with increasing Ag_2Te dispersion concentration dose not originate from the grain boundary scattering of carriers but rather from the decreased electron-electron scattering due to the lower carrier concentration in the 1/1 composite.

The effective mass of the carrier can be calculated by the following relation in a degenerated semiconductor.[32]

$$S = \frac{8\pi^2 \kappa_B^2}{3e\hbar^2} m^* T \left(\frac{\pi}{3n}\right)^{2/3}$$

where m^* and n are the effective mass of the carrier and the carrier concentration, respectively. The effective masses of the ST/AT = 2/1, 4/1, 8/1, and 16/1 composites are almost identical. For the sample of ST/AT = 1/1, the effective mass is significantly lower than the other's effective masses due to the relatively low carrier concentration of the composite.

Sb_2Te_3/ Ag_2Te	n_H ($\times 10^{19}$ cm^{-3})	μ_H (cm^2 V^{-1} s^{-1})	S (μV/K)	m^* (m$_e$)
1/1	2.32	493.770	69.91	0.28
2/1	4.29	283.381	65.61	0.40
4/1	5.67	232.828	58.81	0.43
8/1	5.82	252.039	52.92	0.40
16/1	6.87	234.177	50.81	0.42
32/1	8.96	189.975	48.82	0.49

Table 2 The Hall carrier concentration n_H, Hall mobility μ_H, Seebeck coefficient S, and effective mass m^* of the Sb_2Te_3/Ag_2Te (ST/AT) composites with a molar ratios of (ST/AT = 1/1, 2/1, 4/1, 8/1, 16/1, and 32/1) at 300 K.

The total and lattice thermal conductivity are presented in Fig. 3(c) and 3(d), respectively. The temperature-dependent total thermal conductivity $\kappa(T)$ exhibits decreased values with increasing temperature. Also, the thermal conductivities are found to decrease with increasing Ag_2Te dispersion concentration, this trend is similar to the behaviour of the electrical conductivity. For the ST/AT = 1/1 composite, the $\kappa(T)$ ranges from 0.6~1.4 W m^{-1} K^{-1}, while the ST/AT = 32/1 composite has higher thermal conductivity from 1.6~2.4 W m^{-1} K^{-1}. It was reported that the thermal conductivity value of Ag_2Te have relatively low, in a range of 0.6~0.9 W m^{-1} K^{-1} (Ag_2Te).[27] The thermal conductivity of the single crystalline Sb_2Te_3 compound is 5.6 W m^{-1} K^{-1} along the in-plane direction and 1.6 W m^{-1} K^{-1} in the out-of-plane direction.[34] Polycrystalline bulk Sb_2Te_3 still has a high thermal conductivity of 4.7 W m^{-1} K^{-1}.[35] Accordingly, the decreased thermal

conductivity with increasing Ag_2Te concentration can be understood as resulting from the lower thermal conductivity contribution of Ag_2Te than those of Sb_2Te_3 as well as from the behaviour of the electronic thermal conductivity.
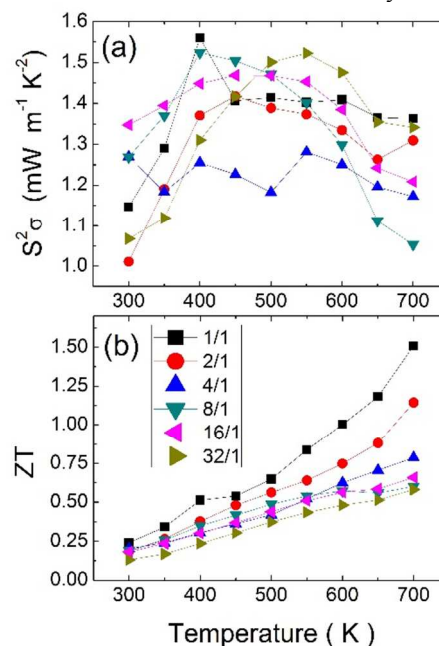
Fig. 4 Temperature-dependent power factor $S^2\sigma$ (a) and ZT values (b) of the Sb_2Te_3/Ag_2Te (ST/AT) composites with molar ratios of (ST/AT = 1/1, 2/1, 4/1, 8/1, 16/1, and 32/1).

Because the thermal conductivity consists of electronic κ_{el} and lattice thermal conductivity κ_{ph}; $\kappa = \kappa_{el} + \kappa_{ph}$, we should subtract the electronic thermal conductivity in order to obtain the lattice thermal conductivity. The electronic thermal conductivity κ_{el} can be calculated by the Wiedemann-Franz law $\kappa_{el} = L_0\sigma T$, where L_0, σ, and T are the Lorenz number, electrical conductivity, and absolute temperature, respectively. In usual cases, the Lorenz number is written as:

$$L_0 = \frac{\pi^2}{3}\left(\frac{k_B}{e}\right)^2 = 2.45 \times 10^{-8} \text{ W }\Omega\text{ K}^{-2}$$

However, the Lorenz number is incorrect in correlated metal and many degenerated semiconductors. In order to obtain a more reliable Lorenz number, we calculated the Lorenz number by using the following equation:[36]

$$L = \left(\frac{k_B}{e}\right)^2 \left(\frac{(r+\frac{7}{2})F_{r+\frac{5}{2}}(\eta)}{(r+\frac{3}{2})F_{r+\frac{1}{2}}(\eta)} - \left[\frac{(r+\frac{5}{2})F_{r+\frac{3}{2}}(\eta)}{(r+\frac{3}{2})F_{r+\frac{1}{2}}(\eta)}\right]^2\right)$$

where r is the scattering parameter, $\eta = E_F/k_BT$ is the reduced Fermi energy, and $F_n(\eta)$ is the n-th order Fermi integral given by

$$F_n(\eta) = \int_0^\infty \frac{x^n}{1+e^{x-\eta}}dx$$

For most cases, the scattering parameter for acoustic phonon scattering is $r = -1/2$. The reduced Fermi energy η can be obtained from a fitting of the Seebeck coefficient to the following equation:

$$S = \pm \frac{k_B}{e} \left\{ \frac{\left(r + \frac{5}{2}\right) F_{r+\frac{3}{2}}(\eta)}{\left(r + \frac{3}{2}\right) F_{r+\frac{1}{2}}(\eta)} - \eta \right\}$$

The calculation result for the Lorenz number by the above equations is shown in the inset of Fig. 3(d). The Lorenz number decreases with increasing temperature in a range of $(1.7\sim2.1)\times10^{-8}$ W Ω K^{-2} which is lower than the value of $L_0 = 2.45 \times 10^{-8}$ W Ω K^{-2}. By subtracting the electronic thermal conductivity $\kappa_{el} = L\sigma T$, the lattice thermal conductivities are in the range of $\kappa_{ph} = 0.1\sim0.7$ W m^{-1} K^{-1}. The lattice thermal conductivity of the Sb_2Te_3 rich composite (ST/AT = 32/1) has a trend similar to that of the stoichiometric one (open star symbol) shown in Fig. 3(d). The lattice thermal conductivities decrease with increasing Ag_2Te dispersion concentration, presumably due to grain boundary phonon scattering. In the case of the ST/AT = 1/1 composite, the extremely low lattice conductivity at high temperature, 0.1 W m^{-1} K^{-1} should be investigated in a further research.

The power factor $S^2\sigma$ and dimensionless figure-of-merit ZT of Sb_2Te_3/Ag_2Te (ST/AT) composites are presented in Fig. 4 (a) and (b), respectively. The power factor shows high values $1.0\sim1.5$ mW m^{-1} K^{-2} with temperature-insensitive behaviour over a wide temperature range; this is an important criterion for practical application in thermoelectric materials. While the power factors are not sensitive to the Ag_2Te concentration, the ZT values increase with increasing of the Ag_2Te dispersion concentration due to decreased thermal conductivity.

The maximum high ZT of 1.5 is reached at 700 K for the ST/AT = 1/1 composite. The ZT = 1.5 at this temperature range is one of the highest values ever recorded in Pb-free p-type thermoelectric chalcogenides. In addition, this value represents a more enhanced value of thermoelectric performance than the ZT value of Ag_2Te related phase separated composites of $Ag_2Te/AgSbTe_2$, which exhibit thermoelectric performance around ZT $1.0\sim1.3$.[16,17] It is very likely that it will be possible to increase the ZT value further by controlling the texture of the composites and the Ag_2Te dispersion concentration then these materials can be practically applied in the field of waste heat power generation as Pb-free p-type thermoelectric materials.

Conclusions

We synthesized Sb_2Te_3/Ag_2Te (ST/AT) composites with molar ratios of ST/AT = 1/1, 2/1, 4/1, 8/1, 16/1, and 32/1 by melting, hand grinding, wet milling, and hot press sintering processes. The low temperature wet milling process can disperse Ag_2Te particles effectively in the Sb_2Te_3 matrix. Thermoelectric property investigation indicated that the Ag_2Te dispersion decreases the electrical conductivity as well as the thermal conductivity reduction. The metallic or semi-metallic behaviour of the composites, because of high electrical conductivity at room temperature and high Seebeck coefficient at high temperature, respectively, gives rise to the temperature insensitive behaviour of the power factor over a wide temperature range. The high power factor over a wide temperature range and the low thermal conductivity are beneficial to increase the ZT value. Thereby, the ZT value reached 1.5 for the ST/AT = 1/1 composite, which is a more enhanced value for related Pb-free chalcogenide thermoelectric

materials. Further investigation of texture and concentration control can increase the ZT value significantly allowing it to reach a level suitable for practical application in waste heat power generation.

Notes and references

[a] Department of Applied Physics and Institute of Natural Sciences, Kyung Hee University, Yongin 446-701, Korea. Fax: +82-31-204-8122, Tel.: +82-31-201-2415, E-mail: jsrhyee@khu.ac.kr
[b] Advanced Electrical Materials Group, Korea Electrotechnology Research Institute, Changwon 641-600, Korea
[c] Department of Materials Science and Engineering, Northwestern University, Evanston 60208, USA

1 J. P. Heremans, V. Jovovic, E. S. Toberer, A. Saramat, K. Kurosaki, A. Charoenphakdee, S. Yamanaka, G. J. Snyder, Nature (London) 2008, **25**, 554.

2 Y. Pei, X. Shi, A. LaLonde, H. Wang, L. Chen, G. J. Snyder, Nature (London) 2011, **473**, 66.

3 K. Biswas, J. He, I. D. Blum, C.-I Wu, T. P. Hogan, D. N. Seidman, V. P. Dravid, M. G. Kanatzidis, Nature (London) 2012, **489**, 414.

4 H. Wanga, J.-H. Bahk, C. Kang, J. Hwang, K. Kima, J. Kim, P. Burke, J. E. Bowers, A. C. Gossard, A. Shakouri, W. Kim, Proc. Nat. Aca. Sci. 2014, **111**, 10949.

5 R. J. Korkosz, T. C. Chasapis, S.-h. Lo, J. W. Doak, Y. J. Kim, C.-I Wu, E. Hatzikraniotis, T. P. Hogan, D. N. Seidman, C. Wolverton, V. P. Dravid, M. G. Kanatzidis, J. Am. Chem. Soc. 2014, **136**, 3225.

6 F. D. Rosi, J. P. Dismukes, E. F. Hockings, Electr. Eng. 1960, **79**, 450.

7 E. A. Skrabek , D. S. Trimmer , CRC Handbook of Thermoelectrics, (Ed: D. M. Rowe) CRC Press LLC , Boca Raton, FL 1995, Ch. 22.

8 C. Woods , Rep. Prog. Phys. 1988, **51**, 459.

9 G. C. Christakudis, S. K. Plachkova, L. E. Shelimova, E. S. Avilov, Phys. Stat. Sol. (a), 1991, **128**, 465.

10 E. M. Levin, S. L. Bud'ko, K. Schmidt-Rohr, Adv. Funct. Mater. 2012, **22**, 2766.

11 B. A. Cook, M. J. Kramer, X. Wei, J. L. Harringa, E. M. Levin, J. Appl. Phys. 2007, **101**, 053715.

12 F. D. Rosi, J. P. Dismukes, E. F. Hockings, Semiconductor Materials for Thermoelectric Power Generation up to 700 ºC, Electrical Engineering, 1960, **19**, 450.

13 H.-J. Wu, S.-W. Chen, T. Ikeda, G. J. Snyder, Acta Mater. 2012, **60**, 1129.

14 P. F. P. Poudeu et al. J. Am. Chem. Soc. 2006, **128**, 14347.

15 Y. K. Koh, C. J. Vineis, S. D. Calawa, M. P. Walsh, D. G. Cahill, Appl. Phys. Lett. 2009, **94**, 153101.

16 S. Yoneda, Y. Ohno, E. Ohta, N. Yuhashi, I. Shiota, Y. Shinohara, H. T. Kaibe, I. J. Ohsugi, I. A. Nishida, IEEJ Trans. FM 2004, **124**, 312.

17 B. Du, H. Li, J. Xu, X. Tang, C. Uher, Chem. Mater. 2010, **22**, 5521.

18 N. A. Heinz, T. Ikeda, Y. Pei, G. J. Snyder, Adv. Func. Mater. 2014, **24**, 2135.

19 Y. Pei, J. Lensch-Falk, E. S. Toberer, D. L. Medlin, G. J. Snyder, Adv. Func. Mater. 2011, **21**, 241.

20 J.-F. Li, J. Liu, Phys. Stat. Sol. (a) 2006, **203**, 3768.

21 Z. He, C. Stiewe, D. Platzek, G. Karpinski, E. Müller, S. Li, M. Toprak, M. Muhammed, J. Appl. Phys. 2007, **101**, 043707.

22 V. Agafonov, N. Rodier, R. Céolin, R. Bellissent, C. Bergman, J. P. Gaspard, Acta Crystal. 1991, **47**, 1141.

23 M. Fujikane, K. Kurosaki, H. Muta, S. Yamanaka, M. Fujikane, K. Kurosaki, H. Muta, S. Yamanaka, J. Alloys & Comp. 2005, **393** 299.

24 P. Loyak, R. Novotnp, J. Horak, J. Klikorka, Phys. Stat. Sol. (a) 1985, **8-9**, K55.

25 G.-H. Dong, Y.-J. Zhu, L.-D. Chen, J. Mater. Chem. 2010, **20**, 1976.

26 Jing Chen et. al., Chem. Mater. 2010, **22**, 3086.

27 M. Fujikane, K. Kurosaki, H. Muta, S. Yamanaka, J. Alloys & Comp. 2005, **393**, 299.

28 H. Scherrer, S. Scherrer, CRC Handbook of Thermoelectrics, (edited by D. M. Rowe) CRC Press, London 1995, p. 239.

29 W. Zhang, R. Yu, H.-J. Zhang, X. Dai, Z. Fang, New J. Phys. 2010, **12**, 065013.

30 H. Zhang, C.-X. Liu, X.-L. Qi, X. Dai, Z. Fang, S.-C. Zhang, Nature Phys. 2009, **5**, 438.

31 W. Zhang, R. Yu, W. Feng, Y. Yao, H. Weng, X. Dai, Z. Fang, Phys. Rev. Lett. 2011, **106**, 156808.

32 G. J. Snyder, E. S. Toberer, Nature Mater. 2008, **7**, 105.

33 P. Zhu, Y. Imai, Y. Isoda, Y. Shinohara, X. Jia, G. Zou, J. Phys. Condens. Matter 2005, **17**, 7319.

34 D. M. Rowe, Thermoelectrics Handbook: Macro to Nano, CRC Press, New York, 2006, Section III, (Chapter 27), p 16.

35 Y. S. Touloukian, D. P. DeWitt, Thermal Conductivity: Metallic Elements and Alloys, IFI/Plenum, New York, 1970.

36 J. H. Kim, M. J. Kim, S. Oh, J.-S. Rhyee, J. Alloys & Comp. 2014, **615**, 933.